RSC Advances

PAPER

View Article Online
View Journal | View Issue

Cite this: *RSC Adv.*, 2024, **14**, 10942

Monophenyl luminescent material with dual-state emission and pH sensitivity for cell imaging†

Yuxin Jin,[a] Bingli Jiang,*[a] Huajian Song,[a] Chanming Mei,[a] Zuoan Liu,[b] Xiakai Zhang,[a] Jinyuan Liu[a] and Yongyang Gong *[b]

Received 24th February 2024
Accepted 26th March 2024

DOI: 10.1039/d4ra01422g

rsc.li/rsc-advances

Dual-state emission (DSE) luminescent materials are a newly discovered category of luminescent materials that exhibit efficient light emission in multiple states, including dilute solutions, highly concentrated solutions, aggregated states and solid states. These materials effectively address the aggregation-caused quenching (ACQ) observed in traditional organic luminescent materials with large conjugated planes, as well as the limitations of aggregation-induced emission (AIE) materials, which typically do not emit light in dilute solutions. The design and development of DSE luminescent materials for organelle imaging applications has attracted considerable interest. In this context, this study presents the design and synthesis of a novel luminescent compound, DMSS-AM, characterised by intramolecular hydrogen bonding and a D–π–A structure. As a monophenyl luminescent material, DMSS-AM exhibits DSE properties with fluorescence quantum yields of 22.1% in solution and 14.0% in the solid state. In particular, it exhibits unique pH-responsive properties, facilitating the targeted detection of lysosomal pH changes. Confocal laser scanning microscopy imaging of cells demonstrated that DSE emitters at both low and high concentrations do not affect image quality for bio-imaging applications. This advance is expected to significantly broaden the applicability of DSE luminescent materials in future applications.

1 Introduction

In almost all cellular activities, the intracellular pH plays a crucial role.[1] A number of important subcellular organelles, such as the mitochondria, the lysosomes and the Golgi apparatus, have different pH distributions and physiological functions within the cell.[2–4] Of these, the lysosome is an acidic organelle with a pH ranging from 4.0 to 6.0. Those acidic pH conditions are necessary for the maintenance of the activity of hydrolytic enzymes in the lysosome. Lysosomes can effectively degrade and digest exogenous biomolecules and perform normal physiological functions under normal pH conditions. The metabolic processes and cellular state of cells can be reflected by changes in lysosomal pH. Typically, pH abnormalities can be the cause of diseases such as cellular dysfunction, neurodegenerative diseases and lysosomal storage disorders.[5,6] Therefore, development of a tool that can effectively track changes in cellular lysosomal pH is essential for keeping track of the metabolic processes and cellular state of the cell.[2,7–9]

Various pH monitoring methods have been developed, including voltammetry, nuclear magnetic resonance (NMR), and spectrophotometry.[10] However, fluorescence spectroscopy is the most widely used method due to its low cost, high sensitivity, fast response, simplicity of operation, and non-invasive detection.[2] Many lysosome-targeted pH-responsive fluorescent probes have been developed.[11–13] The distribution of chemically variable organic fluorescent probes in cell membranes, organelles, and cytoplasm is not well understood due to the complexity of the cellular environment. It is unclear whether they exist as single molecules or in the form of aggregates such as dimers or trimers. The optical properties of organic luminescent materials are greatly affected by different aggregation patterns. For example, molecular probes composed of planar conjugated structures emit light effectively when in a monodisperse state. However, when they aggregate, their quenching properties can potentially have a detrimental effect on the effectiveness of cellular imaging. In contrast, AIE materials exhibit enhanced luminescence efficiency upon aggregation due to limited intramolecular rotation, thereby reducing non-radiative transitions. It is important to note that the size of aggregates has a significant impact on their optical properties.[14–16] Before AIE probes can be used for cellular imaging, they are usually converted into nanoparticles in a tedious process. Therefore, attention has been focused on developing innovative fluorescent probes that maintain optical properties and cellular imaging quality in complex cellular environments, with or without aggregation.

[a]*College of Pharmacy, Guilin Medical University, No. 1 Zhiyuan Rd, Lingui District, Guilin 541199, China. E-mail: jiangbingli@foxmail.com*

[b]*Guangxi Key Laboratory of Optical and Electronic Materials and Devices, College of Materials Science and Engineering, Guilin University of Technology, No. 12 Jian'gan Rd, Qixing District, Guilin 541004, China. E-mail: yygong@glut.edu.cn*

† Electronic supplementary information (ESI) available. CCDC 2329895. For ESI and crystallographic data in CIF or other electronic format see DOI: https://doi.org/10.1039/d4ra01422g

The novel organic luminescent material, currently referred to as dual-state emission (DSE) luminescent materials,[17] combines the advantages of ACQ and AIE active luminescent materials and is effective in dilute solutions, at high concentrations and in the solid state.[18] The unique optical properties of DSE luminophores allow for a wide range of applications in cell imaging.[19,20] Several DSE luminophores have been developed by modification of triphenylamine,[20] phtalamides,[21] benzo[1,2,5]thiadiazole,[22] boron complexes,[23,24] and arenes *et al.* In addition, in recent years, a number of excited-state proton transfer DSE-active luminescent materials have also been reported.[20,25–27] Currently, some DSE luminophores have been used for cellular imaging. However, only a few DES luminophores have been reported for cellular organelles, such as mitochondria, lysosomes, and Golgi apparatus. Therefore, there is a strong need to develop novel DSE luminophores to enable high quality organelle imaging studies.

Small molecule fluorescent probes are highly valued for their ability to easily penetrate cellular membranes of living organisms, allowing for cell imaging without requiring complex preparation techniques.[28] However, fluorescent probes with a single benzene ring structure exhibit low luminescence efficiency, poor colour modulation of luminescence, and require excitation light at energy levels[29] that may be harmful to cells and tissues. There is an urgent need to improve both the brightness and the efficiency of the luminescence in materials that are based on monobenzene rings for bio-imaging purposes. It has been well-documented that adjusting the push–pull electronic properties of donor and acceptor entities within a donor–π–bridge-acceptor (D–π–A) molecular configuration can effectively control the emission colour. Intramolecular hydrogen bonding within the monobenzene luminescent materials can restrict molecular motion, reduce non-radiative transitions and enhance luminescence,[29] as explained by the aggregation-induced emission (AIE) mechanism. Therefore, introducing of the D–π–A structure and intramolecular hydrogen bonding into the single benzene ring structure has the potential to produce luminescent organic materials with DSE properties. These materials meeting the requirements for *in vitro* and *in vivo* bioimaging applications.[28,30,31]

To support our concept, a monophenyl fluorescent probe, termed DMSS-AM (Scheme 1), was developed using dimethyl-2,5-dioxocyclohexane-1,4-dicarboxylate and 2-morpholinoethan-1-amine as synthetic raw materials. This probe has a donor–π–acceptor (D–π–A) configuration and includes intramolecular hydrogen bonding. It is important to note that DMSS-AM is highly soluble in conventional organic solvents and exhibits DSE characteristics. In regards to luminescence efficiency, DMSS-AM achieves 22.1% in aqueous solutions and 14% in solid-state environments. Additionally, it is characterized by robust anti-photobleaching properties, minimal cytotoxicity, and superior biocompatibility. DMSS-AM also exhibits pH sensitivity and can specifically target lysosomes within cells to assess their pH levels. These attributes make DMSS-AM a highly promising candidate for bioimaging applications.

2 Results and discussion

2.1 Synthesis

The synthesis of the target compound DMSS-AM followed the methods reported in previous literature[32] (Scheme S1†). In brief, DMSS-AM was obtained through condensation of dimethyl 2,5-dioxocyclohexane-1,4-dicarboxylate and 2-morpholinoethan-1-amine in a methanol solution using acetic acid as a catalyst. The target compound was investigated single crystal analysis (Fig. S1 and Table S1,† CCDC No. 2329895) and standard spectroscopic methods (Fig. S2–5†). The obtained analysis data corresponded satisfactorily to their molecular structures (see ESI† for detail). The final products exhibit a peak at *m*/*z* 450.34 (calcd: 450.25) in the time-of-flight mass spectrometry (TOFMS) spectra for DMSS-AM (Fig. S5†), confirming the formation of the expected adduct.

2.2 Optical properties in solution

The optical properties of a single benzene-ring organic molecule, DMSS-AM, were investigated in solution. The molecule exhibited absorption and emission wavelengths of approximately 475 nm and 580 nm, respectively, in different solvents (Fig. 1a and b). The

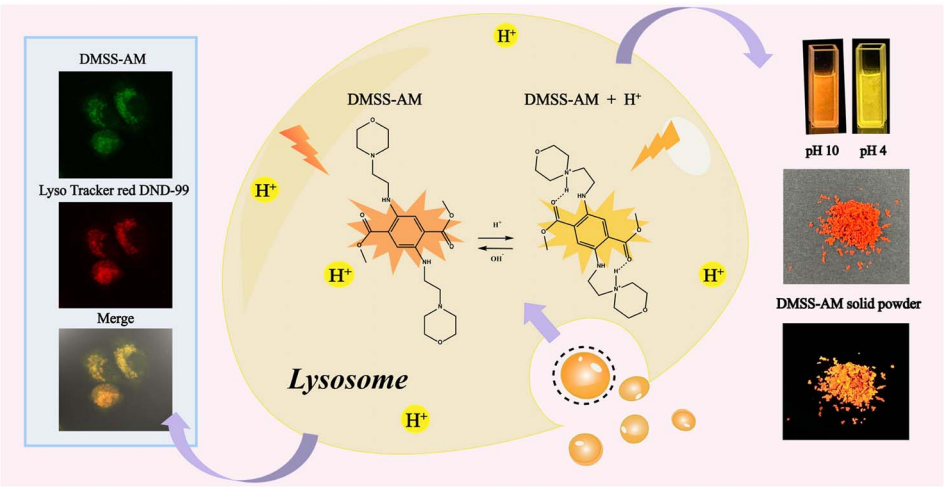

Scheme 1 Chemical structure of DMSS-AM, and its optical properties in solution and solid state, and lysosomal targeting schematic.

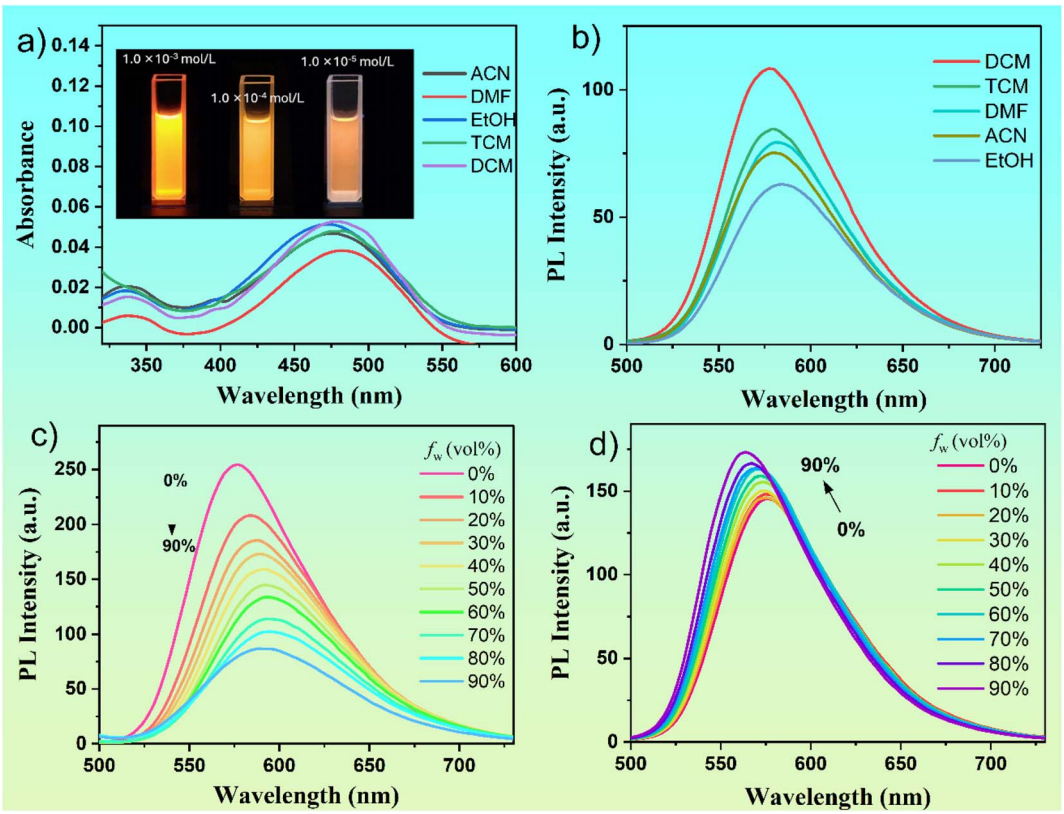

Fig. 1 Absorption (a) and emission (b) spectra of DMSS-AM in different organic solvents, fluorescence emission spectra of DMSS-AM in THF/H_2O mixed solvents with different water contents (c), and in THF/n-hexane solutions with different concentrations (d). The concentration of DMSS-AM is 1×10^{-5} M; The photo inserted in 1a shows the luminescence photo of DMSS-AM at different concentrations under 365 nm UV excitation.

molar extinction coefficients of DMSS-AM in different solvents ranged from ~4.0–5.3 × 10^3 mol L^{-1} cm^{-1}. The polarity of the solvent has little effect on the absorption and emission peak positions but does impact the fluorescence intensity. In solvents such as dichloromethane (DCM), chloroform (TCM), dimethylformamide (DMF), acetonitrile (ACN), and ethanol (EtOH) at a concentration of 1×10^{-5} M, the fluorescence quantum yield of DMSS-AM is denoted as 22.10%, 18.02%, 20.55%, 17.10% and 8.96%, respectively. This indicates that DMSS-AM can effectively emits fluorescence in dilute solutions, overcoming the drawback of AIE compounds not emitting in good solvents and dilute solutions.

The figure inset in Fig. 1a shows that the luminescence intensity of DMSS-AM increases with concentration and does not exhibit an ACQ phenomenon at any concentration. However, as the concentration increases, the fluorescence intensity decreases significantly (Fig. S6†). This indicates that the decrease in fluorescence intensity of DMSS-AM with increasing concentration is due to self-absorption, rather than fluorescence quenching caused by concentration. Under 365 nm UV light excitation, DMSS-AM solid samples exhibit a bright orange-red colour, with a luminescence wavelength of 600 nm (Fig. S7†) and a luminescence efficiency of 14.0%. Therefore, it is evident that DMSS-AM can effectively emit fluorescence in both dilute and high-concentration solutions, as well as in solid states, demonstrating its DSE characteristics.

The photophysical properties of DMSS-AM were investigated in mixed solutions of THF-Water and THF-*n*-hexane. A solvatochromic effect was observed, resulting in a red shift in luminescence with increased water content and a blue shift with rising *n*-hexane content. The photophysical properties of DMSS-AM were investigated in a mixed solution of THF and water. Fig. 1c shows that an increase in water content resulted in a gradual red shift in the luminescence of DMSS-AM, accompanied by a gradual decrease in fluorescence intensity. Conversely, the fluorescence intensity of DMSS-AM in a mixed solution of THF and *n*-hexane increases with the rising content of *n*-hexane (Fig. 1d), while simultaneously displaying a slight blue shift. The solvatochromic effect of D–π–A structured compounds is demonstrated by the luminescence red shift (blue shift) of DMSS-AM in THF-Water (THF-*n*-hexane) mixed solutions as the water (*n*-hexane) content increases. This can be attributed to the enhanced (reduced) polarity of the mixed solvents.

The impact of temperature on the optical properties of organic luminescent compounds is notably significant. To investigate this effect, the emission spectra of dilute DMSS-AM were analysed over a temperature range. The corresponding results of this analysis are presented in Fig. S8.† These observations indicate a gradual and consistent decrease in fluorescence intensity as the temperature increases from 5 to 60 °C. This decline occurs without the presence of any sudden or unexpected shifts in intensity levels, suggesting that hydrogen bond interactions within the diluted DMSS-AM solution are crucial in maintaining the stability of its fluorescence intensity, even as the temperature changes.

2.3 pH sensitive

Under acidic conditions, the tertiary amine in DMSS-AM is protonated to form new hydrogen bonds with the adjacent carbonyl group, resulting in a restriction of molecular motion and a reduction in non-radiative transitions, thereby enhancing luminescence. To investigate the effect of pH on the optical properties of DMSS-AM, The fluorescence spectra of a 1×10^{-4} mol^{-1} L^{-1} DMSS-AM solution were examined at different pH values. Fig. 2 demonstrates that DMSS-AM had the highest fluorescence intensity at pH 4.0, within the pH range of 4.0 to 11.0. However, increasing the pH resulted in a gradual decrease in intensity, particularly at pH values exceeding 8, primarily due to the interruption of intramolecular hydrogen bonding. Fig. 2c shows a nonlinear relationship between fluorescence intensity and pH values within the pH range of 4.0–8.0. However, a strong negative linear correlation ($R^2 = 0.991$) was observed between fluorescence intensity and pH values in the range of 4.8–7.0 (Fig. S9†), demonstrating the DMSS-AM probe's ability to accurately detect pH changes.

Fig. 2a–c clearly shows the fluorescence response of DMSS-AM to pH variations. The fluorescence intensity of DMSS-AM is found to be reversible across the pH range of 4.0 to 7.4, and it is observed that repeated measurements have

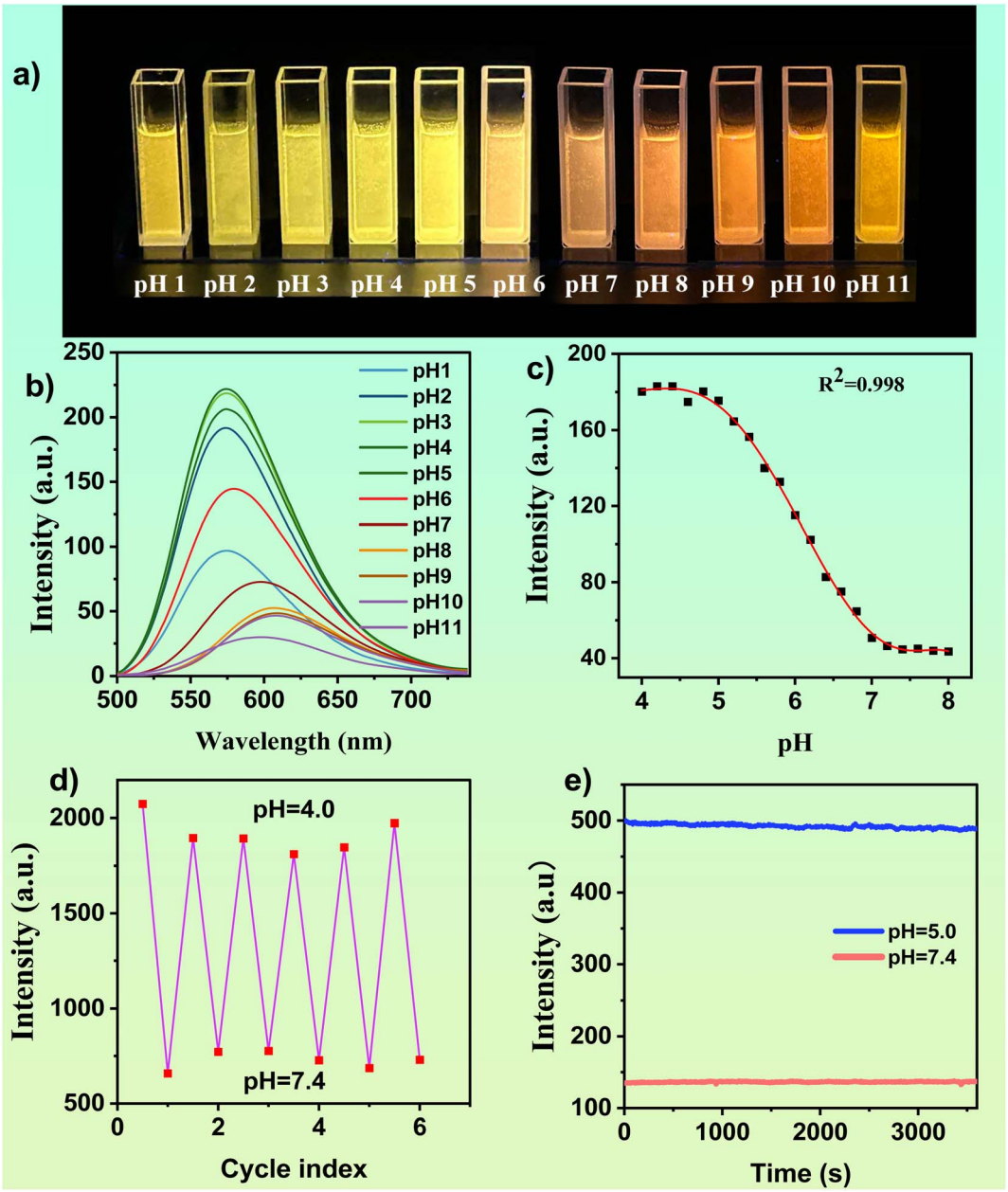

Fig. 2 Photographs of the luminescence of DMSS-AM in different pH environments under excitation by 365 nm ultraviolet light (a). Emission spectra of DMSS-AM in different pH environments (b), and the trend of maximum fluorescence intensity with changing pH values (c). Reversible changes of DMSS-AM in buffer solutions with pH values at 4.0 and 7.4 (d); trend of fluorescence intensity changes over time in buffer solutions with pH values at 5.0 and 7.4 for DMSS-AM (e).

a negligible impact on the intensity levels, as shown in Fig. 2d. This robust and consistent pH-responsive nature of DMSS-AM fluorescence is noteworthy. Photostability is an essential parameter for practical applications. The fluorescence intensity of DMSS-AM was monitored under 468 nm light excitation. The experimental results demonstrate that DMSS-AM exhibits minimal changes in fluorescence intensity over time at pH values of 5.0 and 7.4. These findings indicate the reliability and adaptability of DMSS-AM in maintaining its fluorescence properties under varying environmental conditions, highlighting its potential for practical application in a range of environments.

DMSS-AM is an organic compound that contains ester, secondary amine, tertiary amine, and ether functional groups. It has the potential to form complexes with specific metal ions, which may affect its optical properties. To evaluate the effect of various metal ions on DMSS-AM's optical properties under different pH conditions, fluorescence assessments were conducted in DMSS-AM solutions at pH 5.0 and 7.4 with 18 different metal ions. The fluorescence intensity of DMSS-AM remained stable compared to control samples at both pH levels after the introduction of metal ions, as shown in Fig. S10.† This suggests that DMSS-AM has a strong anti-interference capability with respect to its optical properties in various pH settings, and is minimally affected by the presence of metal ions (Ag^{+}, Ba^{2+}, Ca^{2+}, Co^{2+}, CrO_4^{2+}, Cu^{2+}, Fe^{3+}, K^{+}, La^{+}, Mg^{2+}, Mn^{2+}, Mo^{6+}, Na^{+}, Ni^{2+}, Pb^{2+}, Zn^{2+}, Hg^{2+}, Li^{+}).

2.4 Theoretical calculation

To investigate the pH dependence of DMSS-AM's optical properties, density functional theory (DFT) and time-dependent density functional theory (TD-DFT) were used to investigate the pH dependence of DMSS-AM's optical properties in aqueous solution. The theoretical computational data analysis performed using Multiwfn.[33] The results in Fig. 3c suggest that the vertical excitation process of DMSS-AM in aqueous solution exhibits a typical (n + π) → π* transition. The HOMO and LUMO energy gap are 2.95 eV, and the oscillator strength of vertical excitation is 0.1238. The theoretically calculated absorption peak is approximately at 505 nm, and the corresponding molar extinction coefficient reaches 5.0×10^3 mol L^{-1} cm^{-1} (Fig. S11†). These results suggest that DMSS-AM can efficiently absorb photons and exhibit strong luminescent properties in the solutions state. Fig. 3 illustrates that the intramolecular hydrogen bonding strength in the ground state is −5.33 kcal mol^{-1}.[34] This hydrogen bonding restricts molecular motion, reducing non-radiative transitions and enhancing DMSS-AM's luminescence in dilute solutions. Additionally, the twisted molecular configuration of the compounds prevents π–π interactions in the solid state and at high concentrations (Fig. S1†). This enables efficient light emission in these conditions, as demonstrated in Fig. 1 and S7.†

Under acidic conditions, protonation disrupts the intramolecular –N–H···O=C– plane, leading to an increase in the dihedral angle from 0 to 48.50°. This indicates a reduction in DMSS-AM's degree of conjugation under acidic conditions, which correlates with a blue shift in fluorescence. The N–H···O=C hydrogen bond becomes longer and weaker under acidic conditions compared to neutral conditions. However, protonation also leads to the formation of a new intramolecular hydrogen bond between the adjacent carbonyl group of the quaternary ammonium. This bond has a length of 1.91 Å and a strength of

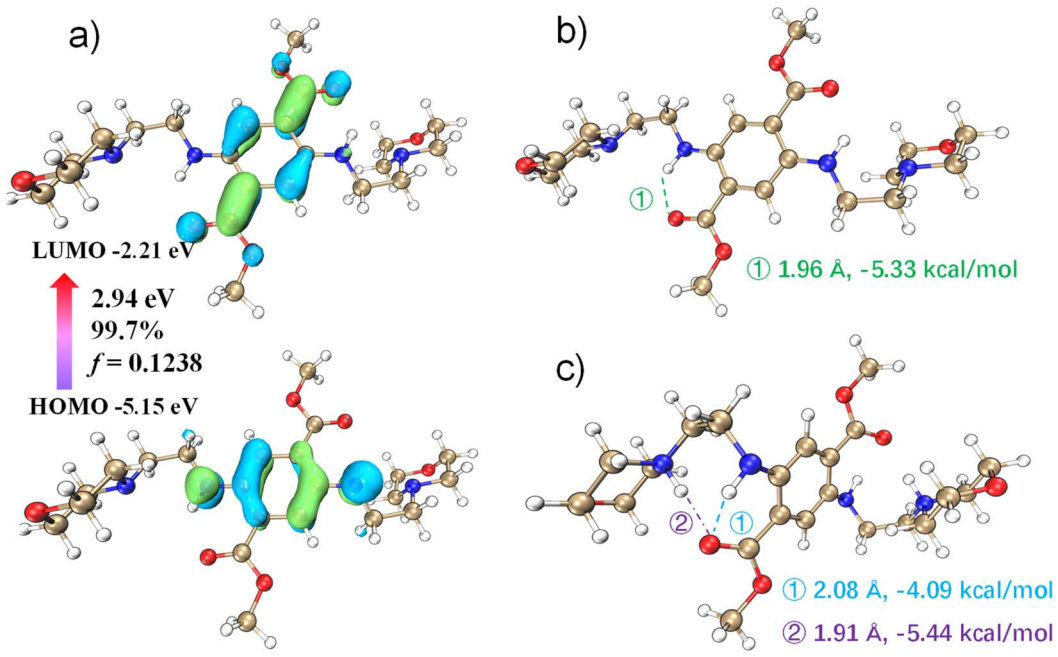

Fig. 3 The frontier molecular orbitals (HOMO and LUMO) of the S_1 state of DMSS-AM in water during the vertical excitation process (a); the molecular configuration, hydrogen bond length, and hydrogen bond strength of DMSS-MA in water under neutral (b) and acidic (c) ground conditions.

−5.44 kcal mol^{-1} (Fig. 3c). As a result, the total intramolecular hydrogen bond strength under acidic conditions is −9.53 kcal mol^{-1} (the sum of the two bond strengths), which is greater than the −5.33 kcal mol^{-1} observed under neutral conditions. Under acidic conditions, DMSS-AM exhibits stronger molecular hydrogen bonding and more,[35] leading to enhanced luminescence, which consistent with experimental observations. These results demonstrate the pH-responsive optical properties of DMSS-AM.

The presence of a flexible morpholine moiety in DMSS-AM makes it challenging to obtain its S_1 molecular configuration, which hinders the in-depth study of its luminescence mechanism. To address this issue, three model compounds, namely dimethyl terephthalate (M1), N^1,N^4-dimethylbenzene-1,4-diamine (M2), and dimethyl 2,5-bis(methylamino)terephthalate (M3), were constructed and used to investigate the luminescence mechanism of DMSS-AM (Fig. 4). The excited state (S_1) properties of these compounds were studied using TD-DFT based on the B3LYP-GD3BJ/6-31G(d) method. Compounds containing amine and ester groups with lone pair electrons are known to undergo n → π* transitions, which facilitate intersystem crossing and the generation of triplet excitons. However, triplet excitons are highly susceptible to quenching by water and oxygen, which often leads to reduced luminescence efficiency or complete non-emission. The TD-DFT study showed that M3 had a significant higher HOMO energy level of M3 compared to M1 and M2. Additionally, M3 had a smaller energy gap of 2.49 eV ($\Delta E_{g(HOMO-LUMO)}$). The theoretical fluorescence emission wavelengths for M1, M2, and M3 in vacuum were calculated to be 384 nm, 389 nm, and 575 nm, respectively (Fig. 4). These results are is consistent with the experimental data.

The HOMO → LUMO transitions of M1 and M2 are significant n → π* transitions, with the proportion of π electrons in their HOMO even lower than 5% (Fig. 4) according to the computational methods reported in previous literature.[36] These transitions share common characteristics of low molar extinction coefficients and low luminescence efficiency. In contrast, M3 exhibits typical π → π* transitions in its HOMO → LUMO transition, with over 95% of π electrons in the HOMO orbital (Fig. 4). The oscillator strength is a crucial physical parameter that characterizes the absorption or emission of luminescent compounds.[37] A transition typically deemed forbidden when the oscillator strength is less than 0.01. Moreover, the oscillator strength is directly proportional to the luminescence efficiency to some extent.[20] Among the three model compounds, M3 has the highest oscillator strength, reaching up to 0.11. Thus, the effective red-orange emission of DMSS-AM, which has a similar structure to M3, can be attributed to its low energy levels, high oscillator strength, and a high proportion of π electrons in the HOMO orbital. Chemical modification has the potential to significantly alter electron distribution, excited state energy, and transition types in the molecule. This enhances luminescence efficiency and facilitates color tuning, making it suitable for use in biomedical imaging, organic electronics, and optoelectronics applications.

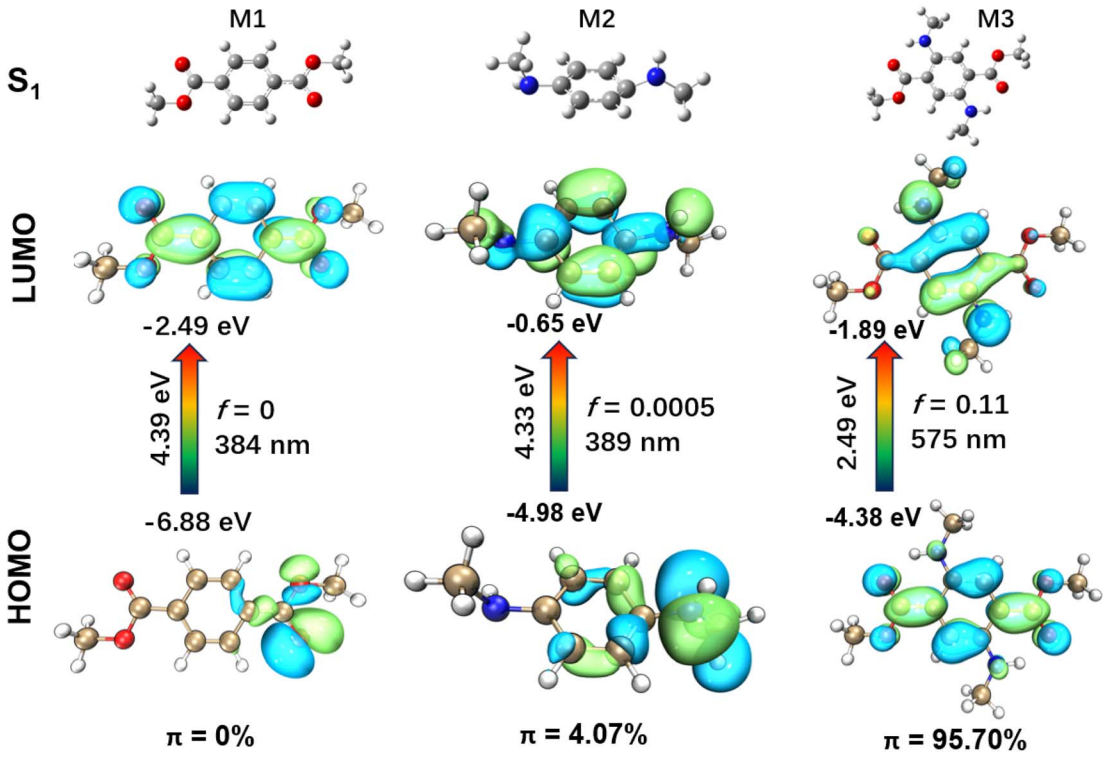

Fig. 4 The molecular configurations and frontier molecular orbitals of three model compounds in the S_1 excited state under gas states, the oscillator strength (*f*) of the $S_1 \rightarrow S_0$ radiative transition, the theoretical fluorescence emission wavelength, and the percentage of π electrons in the HOMO.

2.5 Cell toxicity and cell imaging

DMSS-AM compounds exhibit high luminescence efficiency in both solution and solid states, as well as reversible pH sensitivity, robust resistance to metal ion interference, excellent photostability, and favourable aqueous solubility. These properties make them highly promising in cell imaging. To assess the cytotoxicity of DMSS-AM for cell imaging, a methylthiazolyldiphenyltetrazolium bromide (MTT) assay was conducted. Samples were treated with different concentrations of DMSS-AM (0–50 μM) for 24 hours. The results showed that cell viabilities up to 80% for both HeLa and H_9C_2 cells under experimental conditions when the concentration was lower than 40 μM (Fig. S12†). These findings suggest that DMSS-AM has limited cytotoxicity and is suitable for application in cell imaging.

The dispersion behavior of fluorescent dyes within the complex cellular environment is subject to a multitude of interactions and influences, and as such, remains an unresolved issue. This involves numerous factors, including the chemical structure of the fluorescent dyes, the molecular milieu within the cell, and the various intracellular interactions. During cellular fluorescence imaging, commercial fluorescent dyes should only be used at low concentrations to prevent the adverse effects of ACQ on image quality. Additionally, the optical properties of AIE fluorescent dyes are affected by the degree of aggregation. DSE compounds possess a distinct optical characteristic that enables them to emit light efficiently, regardless of their state (amorphous or crystalline) or concentration. This distinguishes them from ACQ and AIE and gives them a wide range of potential applications in cell imaging.

Fig. 5 displays images captured using a confocal laser scanning microscopy (CLSM) of HeLa cells that were cultured with different concentrations of DMSS-AM for one hour. The results clearly indicate that the cells readily absorb DMSS-AM at various concentrations, and the probe is distributed throughout the lysosomal area. In addition. The green channel (500–540 nm), bright field, and merge channel were recorded. The CLSM images of HeLa cells containing different concentrations of DMSS-AM exhibit strong luminescence. This provides compelling evidence for the effectiveness of DSE luminogens in bioimaging applications, regardless of the concentration being low or high.[38]

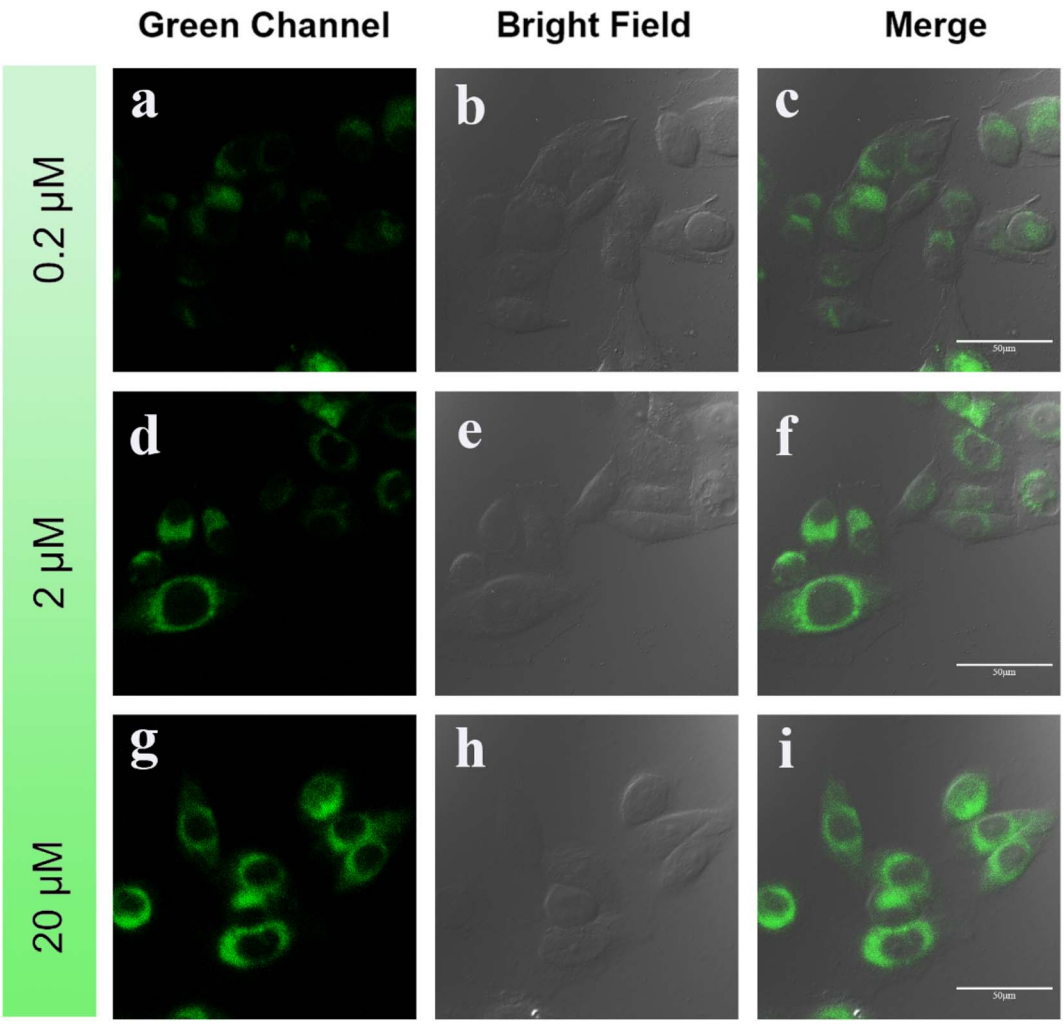

Fig. 5 CLSM images of HeLa cancer cells incubated with different concentrations of DMSS-AM for 1 h, (a, d and g), (b, e and h) and (c, f and i) are green, bright field, and merged channel images, respectively.

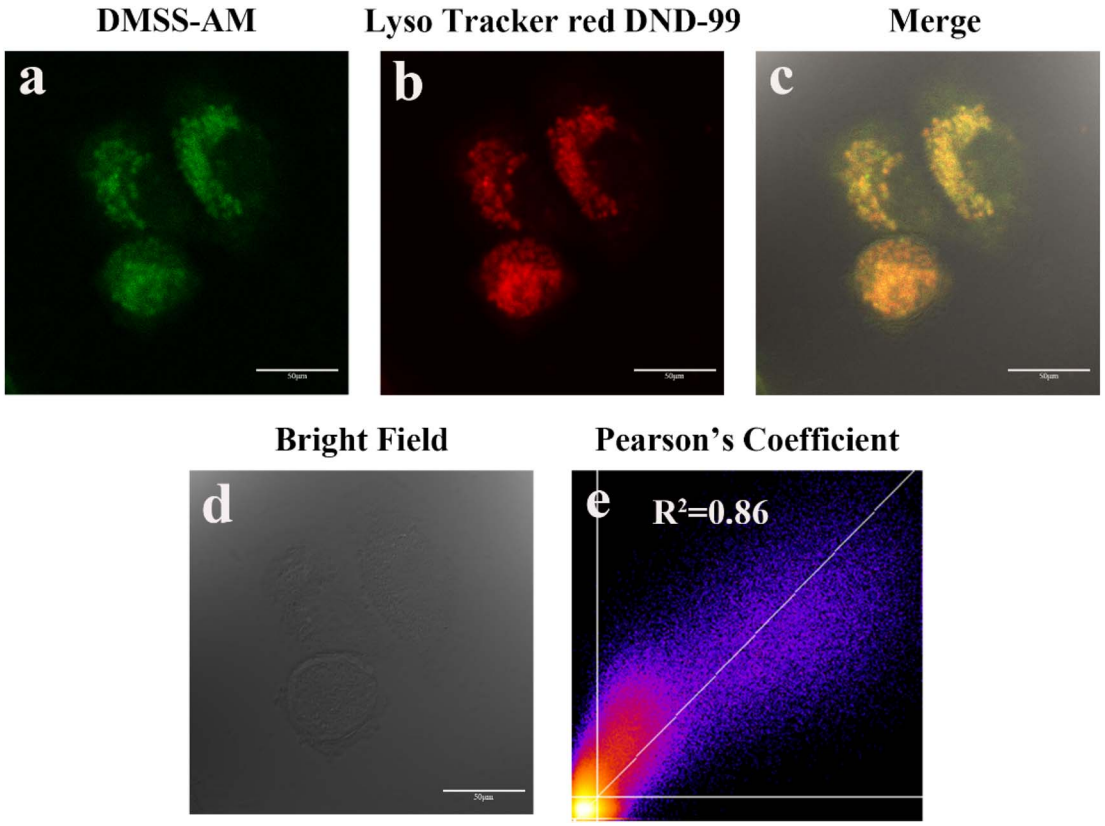

Fig. 6 CLSM images (a–d) of HeLa cells stained with DMSS-AM (20 μM), LysoTracker® Red (70 nM) respectively at 37 °C for 60 min. Cell images collected by green (a), red (b), and merged channel (c) and bright field (d), respectively; (e) scatter plot of fluorescence colocalization of a and b (Pearson's R); the excitation wavelength for green, and red channels are 488 and 561 nm, respectively.

2.6 Targeting lysosomes

Morpholine groups are commonly used to create fluorescent probes for imaging lysosomes. To determine the effectiveness of DMSS-AM, which contains a morpholine moiety, in targeting lysosomes, co-localisation experiments were conducted using the commercial lysosomal fluorescent probe Lyso Tracker red

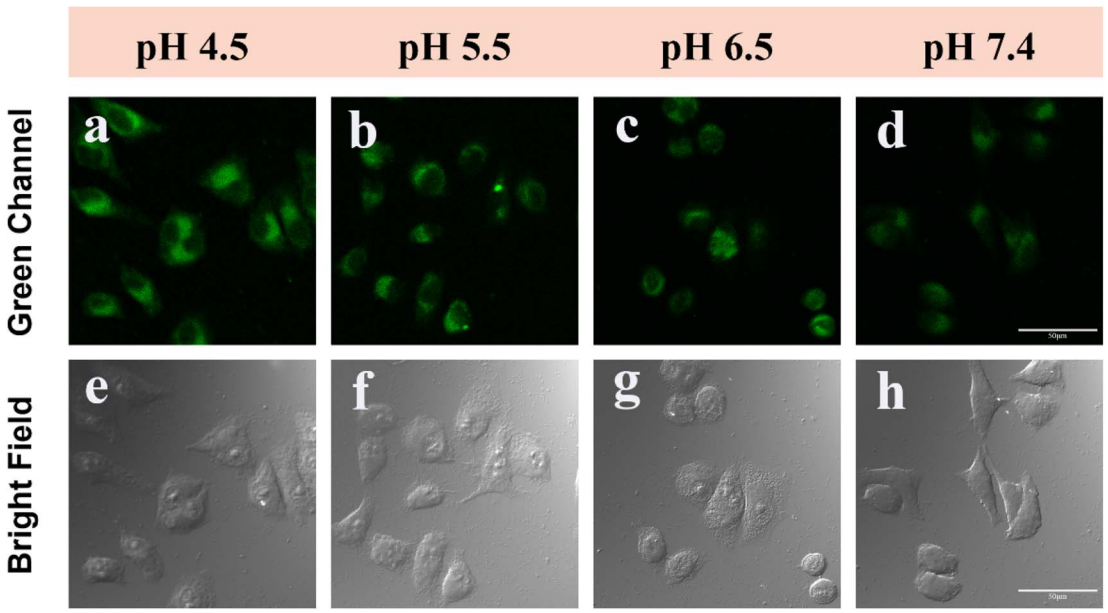

Fig. 7 Green channel (a–d) and bright field (e–h) of CLSM images of HeLa cells stained with DMSS-AM (20 μM, 60 min) incubated for 1 h at 37 °C under different pH condition. λ_{ex} = 488 nm, λ_{em} = 500–540 nm.

DND-99 and DMSS-AM. Fig. 6 presents the results of these experiments. The green (DMSS-AM) and red (Lyso Tracker red DND-99) channels' pseudo-colors showed significant overlap, with a Pearson correlation coefficient of 0.86. This indicates that the distribution of DMSS-AM and Lyso Tracker red DND-99 in HeLa cells is comparable. DMSS-AM selectively localizes in lysosomes within the cellular environment.[39–41]

2.7 Tracking lysosomal pH changes

The effectiveness of DMSS-AM in monitoring intracellular pH changes was assessed by incubating HeLa cells with DMSS-AM under varying pH conditions. The results, as shown in Fig. 7a–h and S13,† indicate that the signal intensity of the CLSM green channel decreased gradually as the pH increased from 4.5 to 7.4. This suggests that DMSS-AM is capable of detecting changes in cellular lysosomal pH. To confirm DMSS-AM's ability to monitor drug-induced alterations in lysosomal pH, HeLa cells were treated with chloroquine and ammonium chloride to manipulate lysosomal pH. Chloroquine, an alkaline antimalarial drug, specifically targets lysosomes and raises their pH, while ammonium chloride, a lysosomal inhibitor, creates an alkaline environment in lysosomes within cells. Fig. S14† shows a significant decrease in signal intensity in the green channel of HeLa cells treated with chloroquine and ammonium chloride. This indicates that DMSS-AM can be used to monitor drug-induced changes in lysosomal pH.

2.8 Photostability of DMSS-AM in cell

This is due to the fact that commercially available lysosomal dyes are susceptible to photobleaching under prolonged exposure to

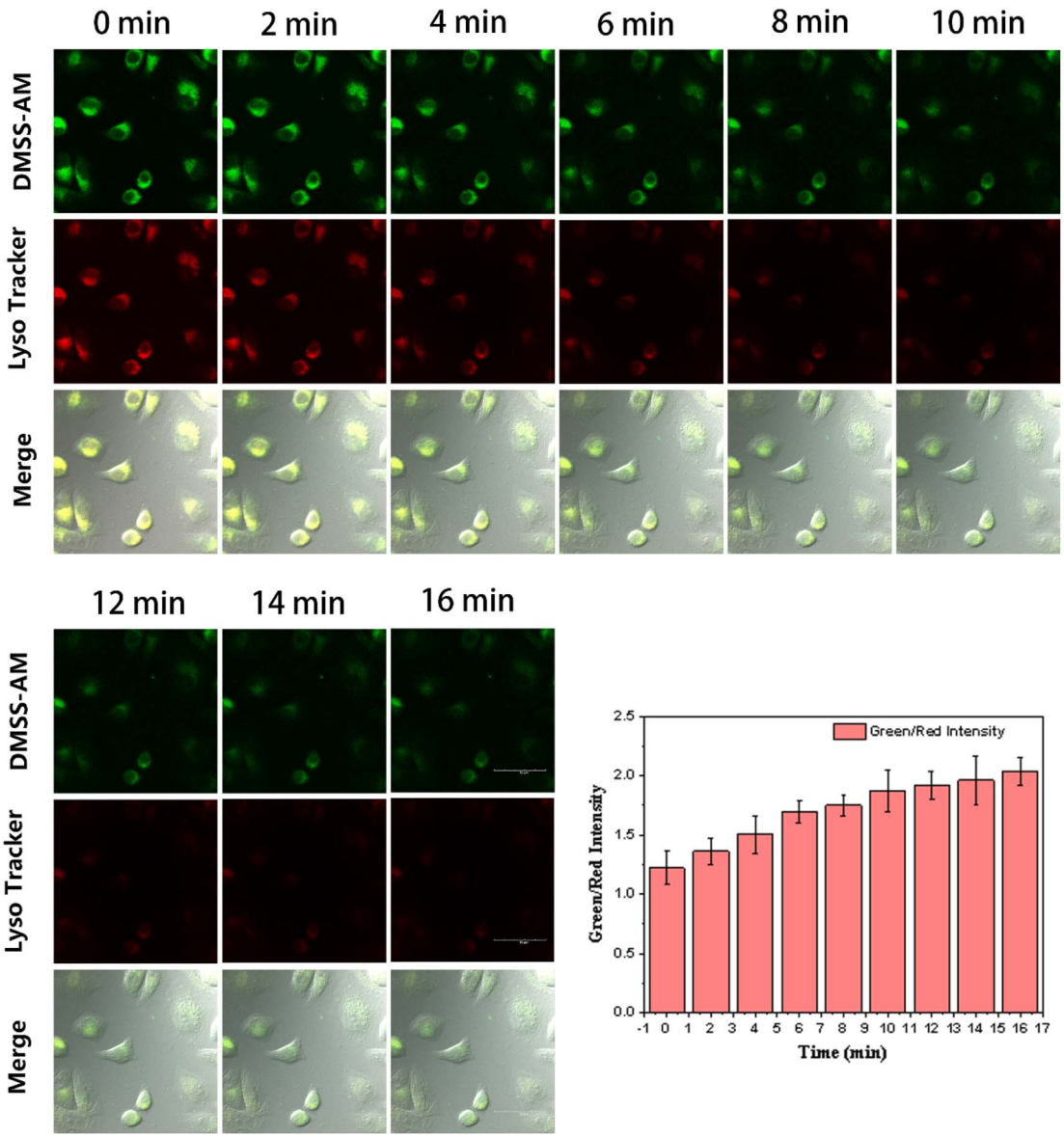

Fig. 8 Imaging of the green and red channels of the CLSM at different times under continuous laser excitation, and the intensity ratio of the green and red channel signals over time.

laser light, which can negatively affect image quality. In the field of cellular imaging, it is crucial to take photostability into account when developing lysosomal fluorescent probes. To assess the photostability of DMSS-AM, HeLa cells were co-stained with DMSS-AM and the commercially available lysosomal marker Lyso Tracker Red DND-99. The co-stained cells were subjected to continuous laser irradiation, and laser confocal microscopy images (LCMS) were captured at various intervals, as depicted in Fig. 8. The signal intensity ratio between the green channel (DMSS-AM) and the red channel (Lyso Tracker Red DND-99) increased gradually with extended laser exposure. The data suggests that DMSS-AM has better photostability than Lyso Tracker Red DND-99. This is evidenced by the relative decrease in signal intensity of the commercially available lysosomal dye in the red channel with prolonged laser irradiation.

3 Conclusion

In conclusion, we have developed a novel pH-sensitive monophenyl chromophore organic luminescent compound, DMSS-AM, based on intramolecular hydrogen bonding and D–π–A structure. This compound exhibits efficient luminescence in both dilute solution and solid states, with a luminescence efficiency of 22.1% in solution and 14% in the solid state. Furthermore, DMSS-AM demonstrates responsive properties to changes in environmental pH. The luminescence intensity gradually increases as the pH decreases within the range of 8.0–4.0, and is accompanied by a blue shift in the emission wavelength. DMSS-AM has excellent membrane permeability and can be used to target lysosomes within cells, allowing for the monitoring of drug-induced lysosomal pH changes. In comparison to commercial lysosome probes, the synthesized DMSS-AM exhibits superior resistance to laser photobleaching. CLSM imaging of cells showed that DSE emitters do not affect image quality at low or high concentrations for bioimaging applications. Additionally, the luminescence efficiency was found to be due to $\pi \rightarrow \pi^*$ transitions, and chemical modification altered the nature of the electronic transitions in the excited state. This provides an experimental basis for designing new efficient luminescent materials. It is believed that these advances will significantly expand the application of DSE luminescent compounds in the future.

Data availability

Additional experimental and characterization data are available in the ESI.† Crystallographic data for compound 1 have been deposited at the Cambridge Crystallographic Data Centre (CCDC) under deposition number 2329895.

Author contributions

Y. J., H. S., C. M. and Z. L. synthesised the substrate, performed the experiments and analysed the data. Y. J., J. L., B. J., X. Z., revised the manuscript. Z. L. acquired NMR data and elucidated the structures. Y. J and B. J. obtained the crystal structure. B. J. and Y. G. supervised the study. Y. G. acquired funding, and revised the manuscript. Y. J., B. J. and Y. G. wrote the manuscript. All the authors have given approval to the final version of the manuscript.

Conflicts of interest

There are no conflicts to declare.

Acknowledgements

This work was financially supported by the National Natural Science Foundation of China (52163017); the Guangxi Natural Science Foundation (2021GXNSFAA220047), the project of Thousand Outstanding Young Teachers' Training in Higher Education Institutions of Guangxi. Innovation and Entrepreneurship Training Program for Students of Guilin Medical University (202310601034).

References

1 G. Miesenböck, D. A. De Angelis and J. E. Rothman, *Nature*, 1998, **394**, 192.
2 J. Han and K. Burgess, *Chem. Rev.*, 2010, **110**, 2709.
3 J. Llopis, J. M. McCaffery, A. Miyawaki, M. G. Farquhar and R. Y. Tsien, *Proc. Natl. Acad. Sci. U. S. A.*, 1998, **95**, 6803.
4 Y. Urano, D. Asanuma, Y. Hama, Y. Koyama, T. Barrett, M. Kamiya, T. Nagano, T. Watanabe, A. Hasegawa and P. L. Choyke, *Nat. Med.*, 2009, **15**, 104.
5 S. Ohkuma and B. Poole, *Proc. Natl. Acad. Sci. U. S. A.*, 1978, **75**, 3327.
6 Q. Wan, S. Chen, W. Shi, L. Li and H. Ma, *Angew. Chem., Int. Ed.*, 2014, **53**, 10916.
7 M. Liu, J. Weng, S. Huang, W. Yin, H. Zhang, Y. Jiang, L. Yang and H. Sun, *Chem. Commun.*, 2023, **59**, 3570.
8 J. Wang, J.-T. Yan, S.-T. Zeng, W. Shao, G.-X. Tang, S.-B. Chen, Z.-S. Huang, J.-H. Tan and X.-C. Chen, *Anal. Chem.*, 2023, **95**, 16609.
9 L. Hu, J. Yang, C. Zhang, J. Pan, S. Shen, L. Su, X. Shen, J. He and H. Wang, *Sens. Actuators, B*, 2024, **398**, 134776.
10 J. Zhou, L. Zhang and Y. Tian, *Anal. Chem.*, 2016, **88**, 2113.
11 H. Xu, Y. Bu, J. Wang, M. Qu, J. Zhang, X. Zhu, G. Liu, Z. Wu, G. Chen and H. Zhou, *Sens. Actuators, B*, 2021, **330**, 129363.
12 A. Mukherjee, P. C. Saha, R. S. Das, T. Bera and S. Guha, *ACS Sens.*, 2021, **6**, 2141.
13 P. Gao, J. Wang, M. Zheng and Z. Xie, *Chem. Eng. J.*, 2020, **381**, 122665.
14 L. Jiang, S. Cao, P. P.-H. Cheung, X. Zheng, C. W. T. Leung, Q. Peng, Z. Shuai, B. Z. Tang, S. Yao and X. Huang, *Nat. Commun.*, 2017, **8**, 15639.
15 W. J. Guo, S. Ma, H. Wang, L. Qiao, L. Chen, C. Hong, B. Liu, X. Zheng and H. Q. Peng, *Aggregate*, 2023, e415, DOI: 10.1002/agt2.415.
16 Y. Zeng, J. Yang and X. Zheng, *Phys. Chem. Chem. Phys.*, 2021, **23**, 23986.
17 J. L. Belmonte-Vázquez, Y. A. Amador-Sánchez, L. A. Rodríguez-Cortés and B. Rodríguez-Molina, *Chem. Mater.*, 2021, **33**, 7160.

18 B. Zhang, L. Wei, X. Tang, Z. Jiang, S. Guo, L. Zou, H. Xie, Y. Gong and Y. Liu, *Materials*, 2023, **16**, 4193.
19 H. Lv, L. Wei, S. Guo, X. Zhang, F. Chen, X. Qin, C. Wei, B. Jiang and Y. Gong, *Front. Chem.*, 2022, **10**, 807088.
20 L. Zou, S. Guo, H. Lv, F. Chen, L. Wei, Y. Gong, Y. Liu and C. Wei, *Dyes Pigm.*, 2022, **198**, 109958.
21 N. Venkatramaiah, G. D. Kumar, Y. Chandrasekaran, R. Ganduri and S. Patil, *ACS Appl. Mater. Interfaces*, 2018, **10**, 3838.
22 G. He, L. Du, Y. Gong, Y. Liu, C. Yu, C. Wei and W. Z. Yuan, *ACS Omega*, 2019, **4**, 344.
23 Y. Qi, Y. Wang, G. Ge, Z. Liu, Y. Yu and M. Xue, *J. Mater. Chem. C*, 2017, **5**, 11030.
24 K. Ohno, F. Narita, H. Yokobori, N. Iiduka, T. Sugaya, A. Nagasawa and T. Fujihara, *Dyes Pigm.*, 2021, **187**, 109081.
25 T. Stoerkler, T. Pariat, A. D. Laurent, D. Jacquemin, G. Ulrich and J. Massue, *Molecules*, 2022, **27**, 2443.
26 M. Durko-Maciag, G. Ulrich, D. Jacquemin, J. Mysliwiec and J. Massue, *Phys. Chem. Chem. Phys.*, 2023, **25**, 15085.
27 J. Luo, G. Song, F. Chen, B. Jiang, L. Wei, Y. Gong, B. Zhang, Y. Liu, C. Wei and B. Z. Tang, *Chem. Eng. J.*, 2023, **454**, 140469.
28 S. Sarkar, A. Shil, Y. W. Jun, Y. J. Yang, W. Choi, S. Singha and K. H. Ahn, *Adv. Funct. Mater.*, 2023, **33**, 2304507.
29 Y. Gong, L. Zhao, Q. Peng, D. Fan, W. Z. Yuan, Y. Zhang and B. Z. Tang, *Chem. Sci.*, 2015, **6**, 4438.
30 H. Kim, Y. Kim and D. Lee, *Acc. Chem. Res.*, 2023, **57**, 140.
31 J. Kim, J. H. Oh and D. Kim, *Org. Biomol. Chem.*, 2021, **19**, 933.
32 B. Tang, C. Wang, Y. Wang and H. Zhang, *Angew. Chem., Int. Ed.*, 2017, **56**, 12543.
33 T. Lu and F. Chen, *J. Comput. Chem.*, 2012, **33**, 580.
34 S. Emamian, T. Lu, H. Kruse and H. Emamian, *J. Comput. Chem.*, 2019, **40**, 2868.
35 Y. Tu, Z. Zhao, J. W. Lam and B. Z. Tang, *Natl. Sci. Rev.*, 2021, **8**, nwaa260.
36 T. Lu and Q. Chen, *Theor. Chem. Acc.*, 2020, **139**, 25.
37 W. Zeng, S. Gong, C. Zhong and C. Yang, *J. Phys. Chem. C*, 2019, **123**, 10081.
38 H. Wu, Z. Chen, W. Chi, A. K. Bindra, L. Gu, C. Qian, B. Wu, B. Yue, G. Liu, G. Yang, L. Zhu and Y. Zhao, *Angew. Chem., Int. Ed.*, 2019, **58**, 11419.
39 S. Cai, C. Liu, X. Jiao, L. Zhao and X. Zeng, *J. Mater. Chem. B*, 2020, **8**, 2269.
40 Z. Liu, Q. Wang, Z. Zhu, M. Liu, X. Zhao and W.-H. Zhu, *Chem. Sci.*, 2020, **11**, 12755.
41 L. Cao, T. Zhu, M. Zan, Y. Liu, X. Xing, Q. Qian, Q. Mei, W.-F. Dong and L. Li, *Sens. Actuators, B*, 2022, **370**, 132424.